Simulations of Ion Thruster Beam Neutralization Using a Particle-Particle Model

Zhao, Yinjian
Wang, Joseph
Usui, Hideyuki

Simulations of Ion Thruster Beam Neutralization Using a Particle-Particle Model

Yinjian Zhao[a] and Joseph Wang[b]
Astronautical Engineering Dept., University of Southern California, Los Angeles, CA

Hideyuki Usui[c]
Department of Computational Science, Kobe University, Kobe, Japan

A Particle-Particle (PP) model is developed to simulate ion thruster beam neutralization by thermal electrons emitted from a neutralizer located outside of the ion beam. Simulations are carried out using the real xenon to electron mass ratio. The results show that beam neutralization is initiated by an electron-ion mixing process in which the thermal electrons are trapped by the potential well in the ion beam and undergo an oscillation between the ion beam boundaries both along the beam direction and in the radial direction. The bouncing of the electrons in the radial direction generates transient oscillating perturbations inside the beam in both electron density and the electric field in the radial direction which eventually dissipate when the electrons are thermalized and the ion beam is neutralized. The PP method directly utilizes the Coulomb's law to calculate the electrostatic force between particles and thus eliminates the constraints on mesh resolution and domain size of the Particle-in-Cell (PIC) method. This method can be advantageous computationally when applied to simulations of very non-uniform, collisionless plasmas such as the plasma plume near ion thruster exit.

[a] Research Assistant. yinjianz@usc.edu
[b] Professor. AIAA Associate Fellow. josephjw@usc.edu. Author to whom correspondence should be addressed.
[c] Professor. h-usui@port.kobe-u.ac.jp

Nomenclature

λ_d = plasma Debye length

ρ_{e0}, ρ_{i0} = electron and ion charge density at the emission surface, respectively

Φ = electric potential

ω_{pe} = plasma frequency

d_e, d_i = size of electron and ion emission surface, respectively

d = gap distance between the electron and ion emission surface

$\vec{E}_i$ = electrostatic field at the location of the ith particle

r_{ij} = distance between two macro-particles

R = radius of finite-sized macro-particle

T_{e0}, T_{i0} = Initial temperatures of the emitted electrons and ions, repectively

v_{di} = ion beam velocity

v_{the} = electron thermal velocity

I. Introduction

Ion thruster beam neutralization is one of the most fundamental aspects of electric propulsion. In an ion thruster, cold beam ions (typical directed flow energy of about 1 keV) are emitted from the thruster exit to provide the thrust and thermal electrons (typical temperature of a few eV) are emitted from a neutralizer to neutralize the ion beam [1]. As the electrons and ions are emitted from separate sources, the ion thruster plume is strongly non-neutral near the thruster exit. However, the electrons and ions couple quickly downstream of the thruster exit to form a quasi-neutral mesothermal plasma plume. One notes that Coulomb collisions are not the primary mechanism for ion beam neutralization because the mean-free path for electron-ion collisions is orders of magnitude larger than the beam size. While beam neutralization can be achieved easily in practice, the precise neutralization process remains unclear.

Ion thruster beam neutralization has been a subject of extensive modeling and theoretical studies [2–14]. The standard method for kinetic simulations of a collisionless plasma is Particle-in-Cell (PIC). Since the electron dynamics play a dominant role in the process, a simulation study of ion

beam neutralization requires the full particle PIC approach where both the electrons and ions are modeled as macro-particles. Early simulation studies of ion beam neutralization considered an infinitely large and uniform beam with thermal electrons premixed with the ions [2–6] and suggested that plasma micro-instabilities and wave-particle interactions may be the driving mechanism for beam neutralization. Recently, several two-dimensional (2-D) and three-dimensional (3-D) full particle PIC simulations considered the emission of a finite size mesothermal plasma plume. Wang et al. [11] considered the emission of beam ions and thermal electrons from the same emission surface. They showed that a potential well is established between the emission source and the propagating beam front, and beam neutralization is achieved through the collisions between the trapped electrons and the potential well along the beam direction rather than micro-instabilities. Yu and Wang [14] considered a simulation setup similar to that of the USC micro-ion thruster[15], which uses a thermionic electron emitter immersed in the ion beam for neutralization. They showed that the macroscopic plume structure exhibits several distinctive regions controlled by the microscopic electron characteristics.

Few existing modeling studies have successfully simulated the typical ion thruster design where the electrons are emitted from a neutralizer located outside of the ion beam. This is primarily due to the constraints on mesh resolution and domain size from a PIC model and the computational cost. A PIC simulation model needs to use a sufficiently fine mesh resolution to resolve the Debye length at the source. In a typical ion thruster design, the dimension of the neutralizer exit, d_e, is much smaller than that of the ion thruster exit, d_i, and the electron density at the neutralizer is much larger than the beam density. Hence, the mesh resolution is controlled by the Debye length at the neutralizer exit. On the other hand, since the beam neutralization process is interwined with the subsequent plume expansion process [11], a PIC simulation of ion beam emission also requires the use of a sufficiently large domain to allow the establishment of a reasonably sized plume in the domain and minimize the effects of domain boundaries on plume expansion [11, 13]. As the ion thruster beam emission is an electrostatic boundary value problem involving both internal and external boundary conditions, one typically needs to use an iterative method to solve the Poisson's equation. The computational time of an iterative Poisson solver increases drastically as the number

of computational cells increases. While the field solve time can be reduced through the use of adaptive mesh, it will still dominate the overall computational time due to the extremely large number of PIC time steps required. This is because the time step in a full particle PIC is determined by the electron time scale, the ion beam simulation must be carried out through many ion plasma periods, and a full particle PIC simulation of such problem must be carried out using a realistic ion to electron mass ratio.

A collisionless plasma may also be simulated using a Particle-Particle (PP) model [16]. A PP model does not use a mesh and calculates the electrostatic forces on particles directly from the Coulomb's law between each particle pair. It is well understood that, in general, the PP method is not as efficient as PIC, because the computing time of PP scales as $O(N^2)$, where N is the number of macro-particles used in the simulation [16]. However, as the PP method eliminates the requirements on mesh resolution and domain size and the need for an iterative field solve, it may provide an attractive alternative to PIC for those applications in which the total computational time is dominated by that of the field solver. In this paper, we explore the application of the PP method to simulate ion beam neutralization.

This paper presents an electrostatic PP model for ion beam neutralization. This simulation model is capable of resolving the ion beam neutralization process for the configuration that emits electrons and ions from separated emission surfaces. Simulations are carried out using real xenon ion to electron mass ratio. Results are presented that show for the first time how thermal electrons emitted from outside of the ion beam mix and neutralize the ion beam. This is the first time that the PP method has been applied to ion propulsion. Section II describes the PP method and compares PP and PIC. Section III discusses PP simulation results. Section IV contains a summary and conclusions.

II. Simulation Model

A. Particle-Particle Model

The PP simulation model presented here is developed for a collisionless plasma with only electrostatic forces. The electrons and ions are modeled by macro-particles. The PP method does not use a mesh. Instead of solving the Poisson's equation on each grid points, the electrostatic field $\vec{E}_i$

at the location of the i^{th} particle is calculated directly from the Coulomb's law

$$\vec{E}_i = \frac{1}{4\pi\epsilon_0} \sum_{j=1, j\neq i}^{N} \frac{q_j}{r_{ij}^3} \vec{r}_{ij} \tag{1}$$

where q_j is the charge of the j^{th} particle, r_{ij} is the distance vector pointing from the j^{th} particle to the i^{th} particle, N denotes total number of macro-particles in the system, ϵ_0 is the permittivity of free space. The dynamics of electrons and ions are solved from

$$\frac{d}{dt}(m\vec{v}) = \vec{F} = q\vec{E}, \quad \vec{v} = \frac{d\vec{x}}{dt} \tag{2}$$

The implementation of particle push is identical to that in a standard PIC code.

One numerical issue in the PP method is that two macro-particles may approach very close to each other within one simulation time step thus resulting in a non-physically large Coulomb's force. Therefore, the implementation of Eq. (1) must be modified in the short range. One approach is to consider that macro-particles are finite-sized rather than point particles and implement a short range force modification to Eq. (1) accordingly. For instance, a simple model in 2-D is to assign the macro-particles a shape of circular disc of radius R with a uniform charge density. The Coulomb's force between two such circular discs can be calculated analytically [17, 18]. Fig. 1 compares the Coulomb's force between two point particles and two circular disc shaped particles as a function of the inter-particle distance in 2-dimension. The radius of the circular particle is R. It shows that, for both the point and circular disc shaped particles, the forces at distance $> 2R$ are the same and obey the Coulomb's law. However, in the short range, the force between the two point particles approaches infinity, while the force between two circular-disc particles approaches zero. The short range force model represented by the circular-disc shaped particle is similar to the quadratic force interpolation scheme used in PIC. One may further simplify the quadratic short range force model into a linear model, which is equivalent to the linear force interpolation scheme used in PIC. The linear short range force model is also shown in Fig. 1. Similar to that used in PIC model, one may choose the size of the particle, $2R$, to be the local plasma Debye length. In this paper, the linear short range force model is used. To save computational time, the results presented in this paper are carried out using a 2-D PP model.

The PP model is applied to two simulation setups shown in Figs. 2 and 3, respectively. The first

setup (Fig. 2) considers that both the ions and the electrons are emitted from the same emission surface. This setup represents ion beam neutralization by a neutralizer immersed inside the ion beam, and is similar to that used in previous full particle PIC simulations in Ref. [11, 13]. The second setup (Fig. 3) considers the emission of ions and electrons from separated surfaces, and is a more accurate representation of the ion thruster configuration used in flight. Here, d_i and d_e denote the size of the ion and electron beam emission surface, respectively, and d denotes the gap between the ion and electron emission source. For the rest of this paper, the following normalization will be used: the velocity, distance, time, and potential will be normalized respectively by v_{the}, λ_d, $1/\omega_{pe}$ and T_{e0}, where $v_{the} = \sqrt{2T_{e0}/m_e}$, T_{e0} is the initial temperature of the emitted electrons, λ_d and ω_{pe} are the Debye length and the electron plasma frequency at the ion emission surface respectively.

B. Particle-Particle vs. Particle-in-Cell

We first compare PP and PIC simulation using the setup of Fig. 2 to validate the PP model. In this comparison, the size of ion beam emission surface d_i and that of the electron emission surface d_e are taken to be $d_i = d_e = 10\lambda_d$, where λ_d is the Debye length at the emission surface. Macro-particles representing the ions and electrons are injected along the x direction from $x = 0$. The ions follow a drifting Maxwellian distribution and the electrons follow a stationary Maxwellian distribution. At the emission surface, the temperature ratio of the injected ions over the injected electrons is taken to be $T_{i0}/T_{e0} = 0.01$, and the drifting velocity of the injected ions is $v_{di}/v_{the} = 0.1$. For this comparison, the simulations were run for a proton plasma with ion to electron mass ratio $m_i/m_e = 1836$. The plasma emitted is a mesothermal plasma. The current density of the injected electrons is taken to be the same as that of the injected ions. Because of the electrons and ions have a very different emission velocity, the plasma is non-neutral immediately downstream of the emission surface. At the emission surface, the initial electron density n_{e0} is much less than the initial ion density n_{i0}.

In the PIC simulation, a uniform mesh with a cell size λ_d is used. The field boundary condition at the emission source is the Dirichlet condition with $\Phi = 0$, The field boundary condition at other outer boundaries is taken to be the Neumann condition with $\frac{\partial \Phi}{\partial n} = 0$. The particle boundary condition at the $x = 0$ surface is reflection and that at all other surfaces are absorption. Through

the use of the zero Neumann boundary condition for the electric field, the potential at the outer boundary of the simulation domain is floating with respect to the thruster exit. This simulates plasma emission in space. At steady state, the potential at the outer domain boundary represents the ambient potential relative to thruster exit. In the PP simulation, the Poisson field solver in PIC is replaced by directly solving the Coulomb's law. The other parts of the code remain unchanged. The particle boundary condition at the $x = 0$ surface is reflection. There are no other boundaries for particles. Hence, the size of the simulation domain is infinite. In both the PP and PIC simulation, the simulation time step is $\Delta t = 0.1\omega_{pe}^{-1}$.

Fig. 4 compares the PIC simulation results with the PP simulation results. The first row shows PIC simulation results and the second and the third row shows PP simulation results. In Fig. 4, the charge density is normalized by the electron charge density at the emission surface $|\rho_{e0}|$, the potential is normalized by the injected electron temperature T_{e0}, and the spatial scale is normalized by the Debye length at the emission surface λ_d. In the PIC simulation, the simulation domain size is $250\lambda_d \times 250\lambda_d$. In both the first and the second row, the number of macro-particles emitted is $N_{in} = 10$ per time step for each species. As the computing of PP scales as $O(N^2)$, in the third row, the number of macro-particles injected per step is reduced to $N_{in} = 2$ for each species to examine the effects of number of macro-particles. We find that the PIC and PP simulations lead to similar results. The minor difference between PIC and PP reflects the effect of mesh resolution on PIC simulation results. The accuracy of field solution in PIC is limited by mesh resolution. In contrast, the PP model is a meshless method. However, for the comparison shown in Fig.4, this minor difference is not significant because the mesh size used in PIC is sufficiently small. Additionally, we also find that reducing the number of macro-particles used in the PP simulation increases the statistical noise but does not change the overall results. Hence, one may use relatively fewer number of particles in a PP simulation to speed up the simulations and still obtain reasonable results.

III. PP Simulations of Ion Thruster Emission with Separated Ion and Electron Sources

In this section, the PP model is applied to simulate the typical ion thruster configuration shown in Fig. 3. The simulation is carried out for a xenon plasma beam, using the real mass ratio of xenon ion to electron $m_i/m_e = 239,560$. The center of the ion beam injection surface is located at $x = 0$

Table 1 Simulation cases.

Case	1	2	3	4	5
d_i/λ_d	100	60	30	100	100
d/λ_d	0	0	0	2	4

and $y = 0$. The electron injection surface is located at $x = 0$ but is separated from the ion emission surface by a distance of d in y. The size of the electron emission surface is taken to be $d_e = \lambda_d$. We consider a range of the parameters d_i and d, as listed in Table 1.

The simulation time step is $\Delta t\omega_{pe} = 0.2$. The simulation is run for $t\omega_{pe} = 1800$. 5 macro-particles representing each species are injected at each time step. The total number of macro-particles is 90000 at the end of the simulation. All other parameters used in the simulation are the same as that used in Sec. II B.

Simulation Case 1 is used as a benchmark case to show the general beam neutralization process. Fig. 5 shows the electron charge density, ion charge density, and potential contours at the end of the simulation $t\omega_{pe} = 1800$. Although the electrons are emitted from outside of the ion beam, a quasi-neutral plume is formed quickly downstream of the ion beam emission surface. The separation of the electron and ion emission source causes a slight asymmetry in the potential contours in the y direction. Notice that, for this simulation, the beam keeps focused and has no divergence in the y direction. This is because all the beam ions are emitted along the x direction with no initial beam divergence and the xenon ions are too heavy to undergo noticeable expansion in the y direction during the time period of the simulation. (For comparison, simulations carried out using the proton ion to electron mass ratio show significant ion beam divergence in Fig. 3.)

Previous PIC simulations have studied the beam neutralization process after the electrons and ions have mixed together in the beam. Simulations of ion beam neutralization by a neutralizer immersed in the beam showed that a potential well is established between the thruster exit and the ion beam front which traps electrons. The primary mechanism for beam neutralization is through the collisions between the trapped electrons and the potential well along the beam direction. The interaction process along the beam direction was discussed in detail in Ref.[11, 13, 14]. For the

setup considered here, placing the neutralizer outside of the ion beam does not affect the process along the beam direction but introduces an additional process perpendicular to the beam direction. Hence, we next study the initial electron-ion mixing process and focus on the electron dynamics in the direction perpendicular to the beam.

Fig. 6 shows the time history of the phase space (v_y vs. y) for a group of electrons injected during the time period of $t\omega_{pe} = 1$ to $t\omega_{pe} = 140$. The results show that, after injection from the neutralizer, the electrons will be first accelerated in the $-y$ direction towards the ion beam. Once inside the ion beam, trapped by the potential well created by the ion beam, the electrons start to bounce between the boundaries of the ion beam in the y direction in addition to collisions with the potential well in the beam direction. The electron bouncing movement in the y direction eventually disappears and the electrons are thermalized. For this simulation setup, electron thermalization along y is completed at $t\omega_{pe} \sim 1000$ ($t\omega_{pi} \sim 2$).

To further study the electron-ion mixing process, Fig. 7 shows the transient time history of the local electron density profile along the y direction, $n_e(y,t)$, as well as snapshots of $n_e(y,t)$ at 4 selected time steps. The electron density plotted are for the region $0 < x/\lambda_d < 20$ and $-60 < y/\lambda_d < 60$. We find that an oscillation pattern appears in the $n_e(y,t)$ time history plot. Fig. 8 shows the time history of the local electrostatic field component $E_y(y,t)$, where $E_y(y,t)$ is plotted for a line perpendicular to the beam direction located at $x/\lambda_d = 10$, $-100 < y/\lambda_d < 100$. It is interesting to note that a similar oscillation pattern also appears in the $E_y(y,t)$ time history plot.

The oscillation pattern shown in Figs. 7 and 8 suggests the following process in the direction perpendicular to beam emission. For the 2-D simulation setup shown in Fig. 3, we shall refer the beam boundary at $y/\lambda_d = 50$ as the upper beam edge, and that at $y/\lambda_d = -50$ as the lower beam edge. In Case 1, the electrons are emitted from just outside the upper edge. Immediately after the start of ion beam emission at $t = 0$, a high positive potential is established inside the beam. The electrons emitted from outside the upper edge are accelerated by this high potential to enter into the ion beam. Once inside the beam, the electrons are trapped by the potential well. As the initial group of electrons reaches the lower beam edge, the deceleration and reflection of electrons

create an enhancement in n_e at the lower edge. This electron dynamics generate a perturbation wavefront in electron density, which propagates first in the $-y$ direction and then is reflected back in the $+y$ direction by the lower beam edge. Subsequent electron emission and propagation create the n_e enhancement at both the lower and upper beam edges, and thus two perturbation wavefronts bouncing between the beam edges. One can expect that each reflection at the beam edge further breaks the wavefront into smaller perturbations. The oscillating perturbation in $n_e(y)$ generates a similar oscillation patten in the electric field component $E_y(y)$ along the y direction. As the ion beam becomes more neutralized, both the magnitude of E_y inside the beam and the electron density peak at beam boundary start to decrease. Hence, the oscillating perturbation of $n_e(y)$ and $E_y(y)$ in the y direction is a transient process which eventually dissipates. As Fig. 7 shows, the $n_e(y)$ profile becomes near uniform in y inside the beam at $t\omega_{pe} >\sim 1000$.

The transient perturbation along the y direction may also be investigated by applying the fast Fourier transform (FFT) on E_y. The top pane of Fig. 9 shows the FFT of $E_y(y)$ at $(x/\lambda_d, y/\lambda_d) = (10, 50)$ for the time period of $200 < \omega_{pe}t < 1800$ for Case 1. The FFT spectrum shows two peak frequencies, denoted as f_1 and f_2 respectively. Note that f_1 corresponds to the oscillation at $200 < \omega_{pe}t < 600$ and f_2 corresponds to the oscillation $600 < \omega_{pe}t < 1800$ shown in Fig. 8, respectively. We further obtained the average speed in the y direction for the electrons in the region $0 < x < 20$ and $-\frac{d_i}{2} < y < \frac{d_i}{2}$, $< |v_y| >$ (Fig. 10). From f_1, f_2, and $< |v_y| >$, one can estimate the average oscillation length associated with the bouncing of electron density perturbation between the beam edges in the y direction. For Case 1, the oscillation length associated with f_1, L_1, can be estimated as

$$\frac{L_1}{\lambda_d} = \frac{< |v_y| >_1}{f_1 \lambda_d} \approx \frac{1.35}{0.0589} \frac{2\pi v_{the}}{\omega_{pe}\lambda_d} \approx 203.71 \approx 2d_i \tag{3}$$

and the oscillation length associated with f_2, L_2, can be estimated as

$$\frac{L_2}{\lambda_d} = \frac{< |v_y| >_2}{f_2 \lambda_d} \approx \frac{1.5}{0.1336} \frac{2\pi v_{the}}{\omega_{pe}\lambda_d} \approx 99.79 \approx 1d_i \tag{4}$$

where $< |v_y| >_1$ and $< |v_y| >_2$ are obtained from macro-particles representing electrons for the corresponding time periods (Fig. 10). This suggests that the first peak, f_1, is associated with one n_e wavefront bouncing between the beam edges as L_1 is approximately the round-trip length

$(2d_i)$ across the beam in the y direction. Similarly, the second peak, f_2, is associated with two n_e wavefronts moving across each other in the y direction within the beam as $L_2 \simeq d_i$. The frequencies associated with the oscillations of more n_e wavefronts are too weak to show up in the FFT spectrum.

We further carried out simulations using different values of d_i and d. The FFT results of E_y are also compared in Fig. 9. Carrying out the same estimation using Eq. (3) and Eq. (4) for Cases 2-5, we find that all the cases exhibits the same transient process. The results also show that when the beam size d_i decreases, the oscillation frequency will increase, and $< |v_y| >$ will decrease. Hence, for the simulation setup considered here, the electrons emitted from outside the ion beam creates a propagating n_e wavefront in the y direction inside the beam. The n_e perturbation oscillates between the beam edges and dissipates each time it is reflected until $n_e(y)$ eventually becomes near uniform inside the ion beam.

IV. Summary and Conclusions

A PP model, which directly utilizes the Coulomb's law to calculate the electrostatic force between charged particles, is developed to simulate ion thruster beam neutralization. The PP method eliminates the requirements on mesh resolution and domain size and thus may provide an attractive alternative to the PIC method on simulations of non-uniform collisionless plasmas. In particular, it can be advantageous when applied to those applications in which the total PIC simulation time is dominated by that from an iterative Poisson solver. The PP model is applied to simulate ion thruster beam neutralization for a setup in which cold beam ions and thermal electrons are emitted from separate emission sources. Simulations are carried out using the real xenon ion to electron mass ratio. Results are presented that show for the first time how thermal electrons emitted from outside of the ion beam mix and neutralize the ion beam. Once thermal electrons are attracted by the potential well inside the ion beam, they will undergo oscillations both along and perpendicular to the beam direction. The oscillations along the beam direction are between the sheath formed at the ion thruster emitting surface and the propagating beam front, and was also observed in previous simulations of ion beam neutralization by thermal electron emission from a neutralizer immersed in the ion beam[11, 14]. Placing the neutralizer outside of the ion beam generates additional oscillations in the radial direction. The bouncing of the trapped electrons in the radial direction generates

transient oscillating perturbations in both electron density and the radial electric field component in the radial direction inside the beam. The perturbation starts as a single wavefront and dissipates into more wavefronts as they are reflected at the beam boundary. The oscillating perturbations in the radial direction eventually dissipate when the electrons are thermalized and the ion beam is neutralized.

Acknowledgments

We acknowledge useful discussions with Y. Hu.

References

[1] Wang, J., Brinza, D., and Young, M., "Three-dimensional Particle Simulations of Ion Propulsion Plasma Environment for Deep Space 1," *Journal of Spacecraft and Rockets*, Vol. 38, No. 3, 2001, pp. 433–440. doi:10.2514/2.3702.

[2] Buneman, O. and Kooyers, G. P., "Computer Simulation of the Electron Mixing Mechanism in Ion Propulsion," *AIAA Journal*, Vol. 1, No. 11, 1963, pp. 2525–2528. doi:10.1524/3.2104.

[3] Buneman, O., "Maintenance of Equilibrium by Instabilities," *Journal of Nuclear Energy*, Vol. 2, 1961, pp. 119–134. doi:10.1088/0368–3281/2/1/320.

[4] Derfler, H., "Nonexistence of Quiescent Plasma States in Ion Propulsion," *Physics of Fluids*, Vol. 7, 1964, pp. 1625–1637. doi:10.1063/1.1711068.

[5] Dunn, D. A. and Ho, I. T., "Longitudinal Instabilities in an Electrostatic Propulsion Beam with Injected Current Neutrality," *Internaltional Electric Propulsion Conference*, , No. IEPC 1963-41. doi:10.2514/6.1963-41, 1963.

[6] Wadhwa, R. P., Buneman, O., and Brauch, D. F., "Two-Dimensional Computer Experiments on Ion-Beam Neutralization," *AIAA Journal*, Vol. 3, No. 6, 1965, pp. 1076–1081. doi:10.2514/3.3057.

[7] Othmer, C., Glassmeier, K. H., Motschmann, U., Schule, J., and Frick, C., "Three-Dimensional Simulations of Ion Thruster Beam Neutralization," *Physics of Plasmas*, Vol. 7, 2000, pp. 5242–5251. doi:10.1063/1.1322060.

[8] Othmer, C. and Glassmeier, K. H., "Numerical Parameter Studies of Ion-Thruster-Beam Neutralization," *Journal of Propulsion and Power*, Vol. 19, 2003, pp. 953–963. doi:10.2514/2.6189.

[9] Wheelock, A., Cooke, D. L., and Gatsonis, N. A., "Investigation of Ion Beam Neutralization Processes with 2-D and 3-D PIC Simulations," *Computer Physics Communications*, Vol. 164, 2004, pp. 336–343.

doi:10.1016/j.cpc.2004.06.045.

[10] Brieda, L. and Wang, J., "Modeling of Ion Thruster Beam Neutralization Using a Fully Kinetic ES-PIC Code," *41st AIAA/ASME/SAE/ASEE Joint Propulsion Conference*, No. 2005-4045, Tucson, Arizona, USA, July 2005.

[11] Wang, J., Chang, O., and Cao, Y., "Electron-Ion Coupling in Mesothermal Plasma Beam Emission," *IEEE Transactions on Plasma Science*, Vol. 40, No. 2, 2012, pp. 230–236. doi:10.1109/TPS.2011.2179066.

[12] Usui, H., Hashimoto, A., and Miyake, Y., "Electron behavior in ion beam neutralization in electric propulsion: full particle-in-cell simulation," *Journal of Physics: Conference Series*, Vol. 454, 2013. doi:10.1088/1742-6596/454/1/012017.

[13] Hu, Y. and Wang, J., "Electron Properties in Collisionless Mesothermal Plasma Expansion: Fully Kinetic Simulations," *IEEE Transactions on Plasma Science*, Vol. 43, No. 9, 2015, pp. 2832–2838. doi:10.1109/TPS.2015.2433928.

[14] Hu, Y. and Wang, J., "Fully Kinetic Simulations of Collisionless Mesothermal Plasma Emission: Macroscopic Plume Structure and Microscopic Electron Characteristics," *Physics of Plasmas*, Vol. 24, No. 3, 2017, pp. 035510. doi:1.1063/1.4978484.

[15] Polansky, J., Wang, J., and Ding, N., "Experimental Investigation on Plasma Plume Potential," *IEEE Transactions on Plasma Science*, Vol. 41, No. 12, 2013, pp. 3438–3447. doi:10.1109/ TPS.2013.2277724.

[16] Hockney, R. W. and Eastwood, J. W., *Computer Simulation Using Particles*, IOP Publishing Ltd, New York, NY, 1988.

[17] Dawson, J. M., "Particle Simulation of Plasmas," *Reviews of Modern Physics*, Vol. 55, 1983, pp. 403. doi:10.1103/RevModPhys.55.403.

[18] Okuda, H. and Birdsall, C. K., "Collisions in a Plasma of Finite-Size Particles," *Physics of Fluids*, Vol. 13, 1970, pp. 2123–2134. doi:10.1063/1.1693210.

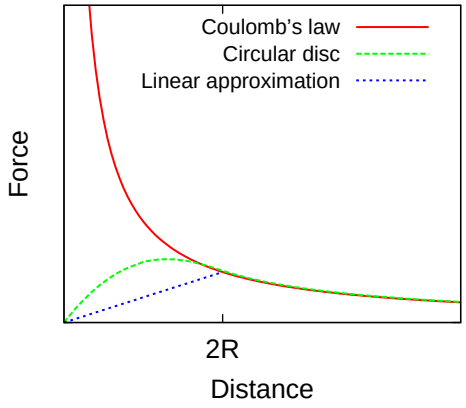

Fig. 1 Comparison of the Coulomb force models: two point particles vs. two finite-sized particles.

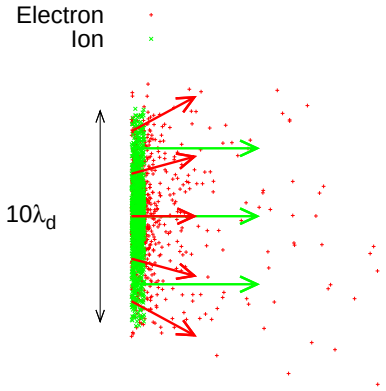

Fig. 2 Simulation setup 1: ions and electrons emitted from the same emission location.

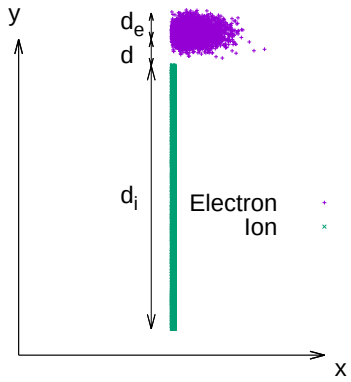

Fig. 3 Simulation setup 2: ions and electrons emitted from separated emission locations.

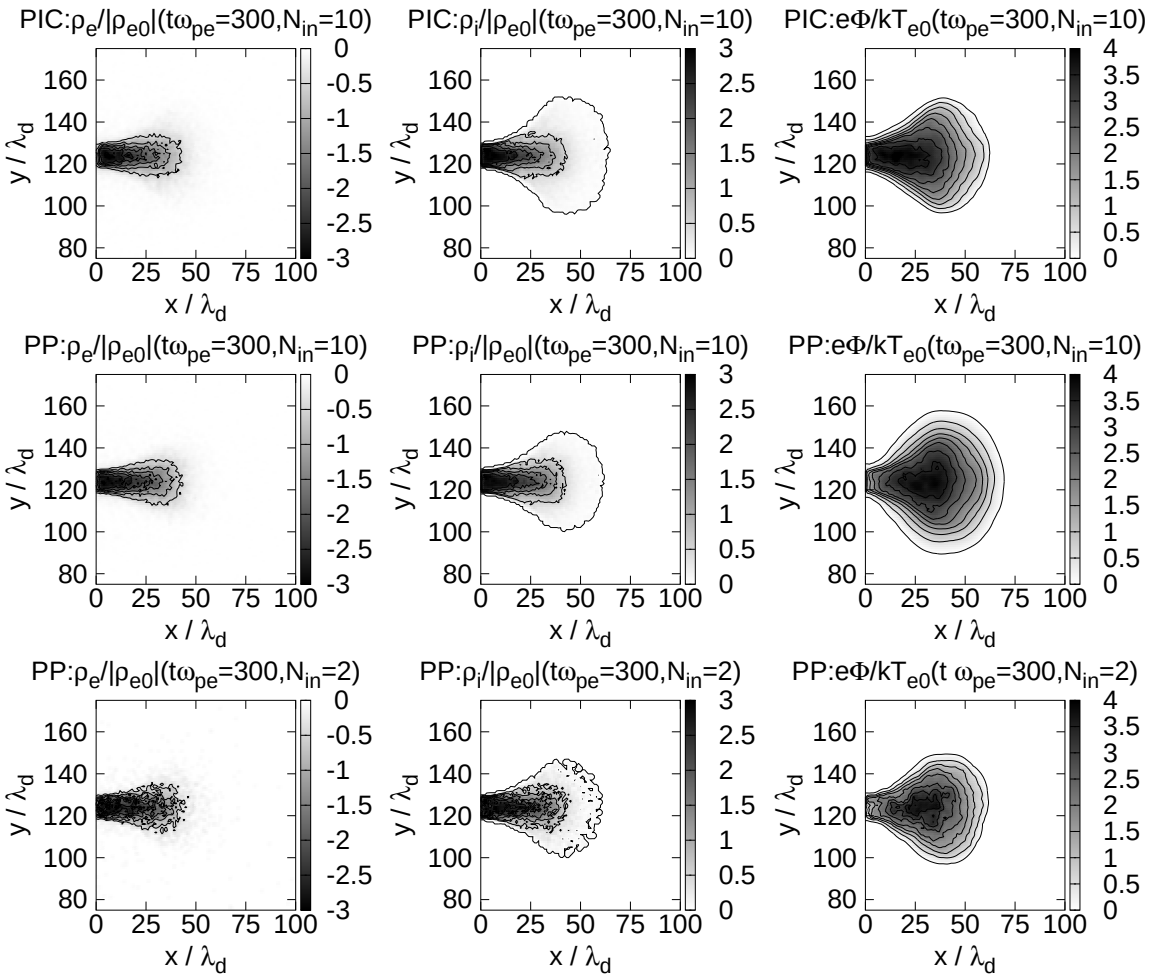

Fig. 4 Comparisons of PIC and PP: electron charge density contours (left) , ion charge density contours (middle), and potential contours (right).

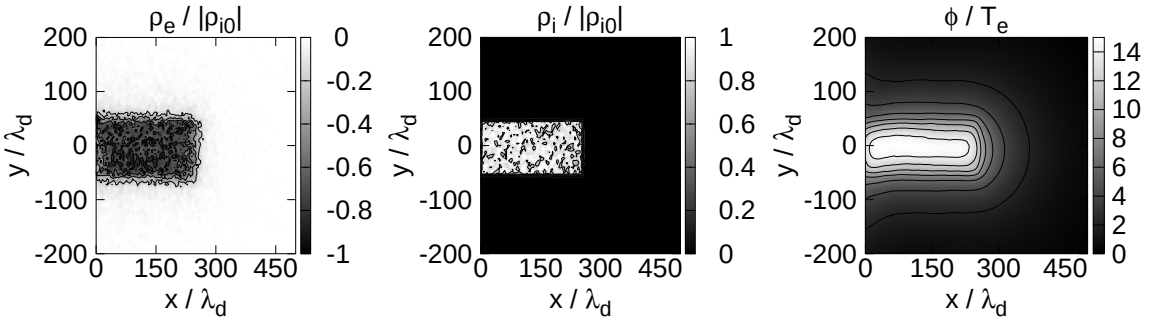

Fig. 5 Case 1: Electron charge density, ion charge density and potential contours at $t\omega_{pe} = 1800$.

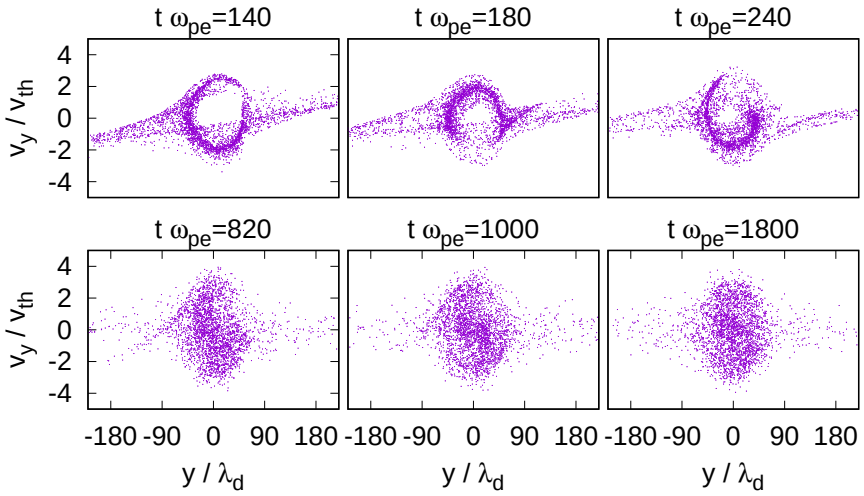

Fig. 6 Case 1: Phase space plots for electrons injected from $t\omega_{pe} = 1$ to $t\omega_{pe} = 140$.

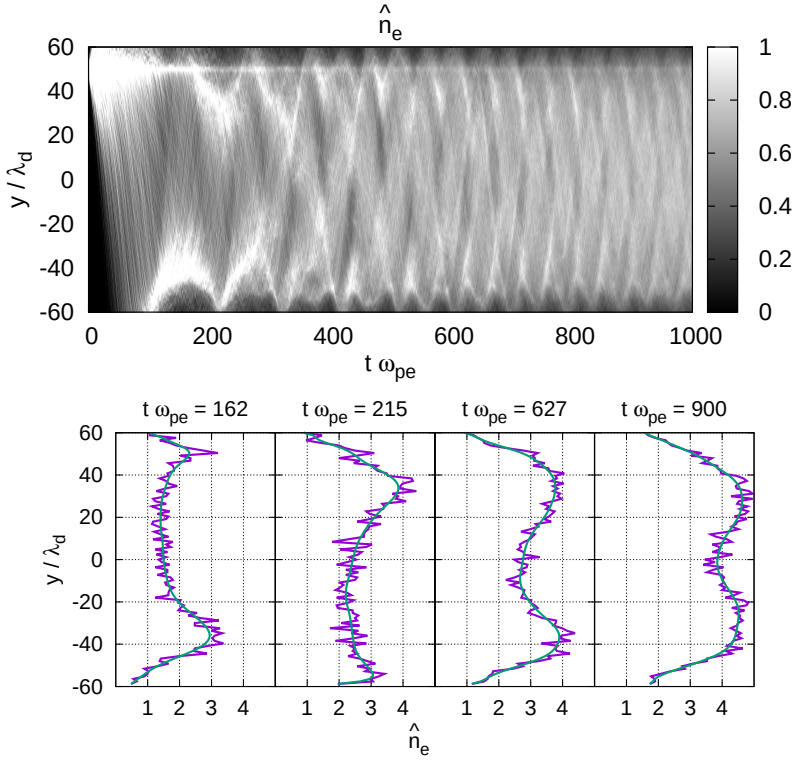

Fig. 7 Case 1: time history of local electron density $\hat{n}_e$ averaged for the region $(0 < x/\lambda_d < 20, -60 < y/\lambda_d < 60)$ (top) and snapshots of 1D profile of of $\hat{n}_e$ at several time steps (bottom). (The $\hat{n}_e$ profile is plotted with a spatial resolution of $\sim \lambda_d$ and is overlaid with a smoothed profile for clarification)

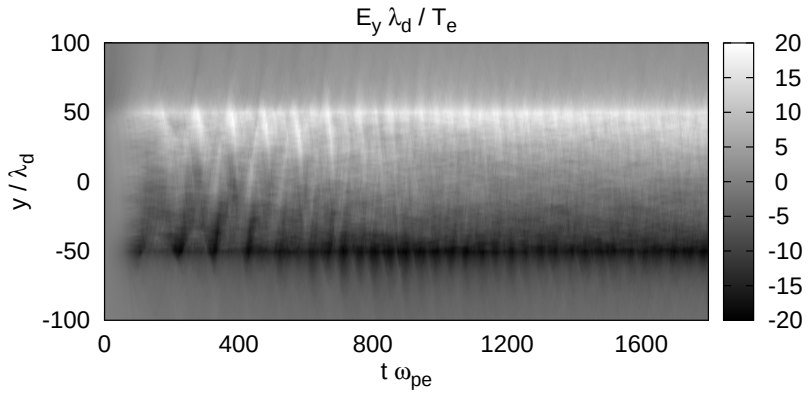

Fig. 8 Case 1: Time history of the transverse electric field component E_y on a line at $(x/\lambda_d = 10, -100 < y/\lambda_d < 1000)$.

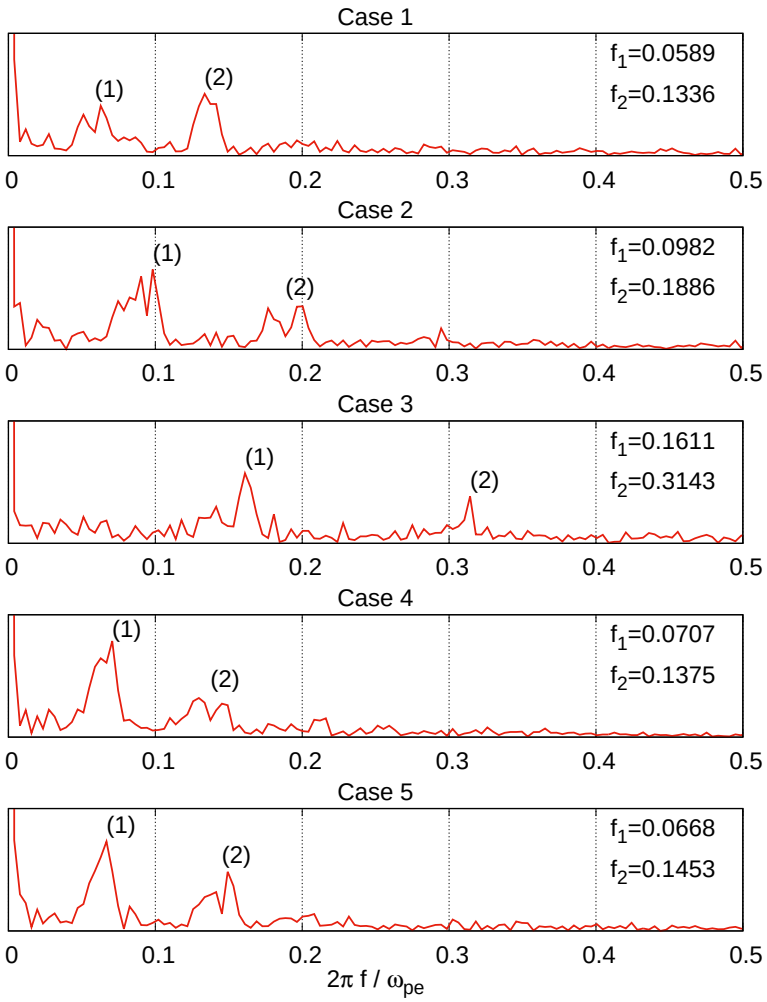

Fig. 9 Case 1 through 5: Results from fast Fourier transforms of $E_y(t)$ at location $(x/\lambda_d, y/\lambda_d) = (10, d_i/2)$ ($d_i/2$ denotes the location of the beam edge in y direction).

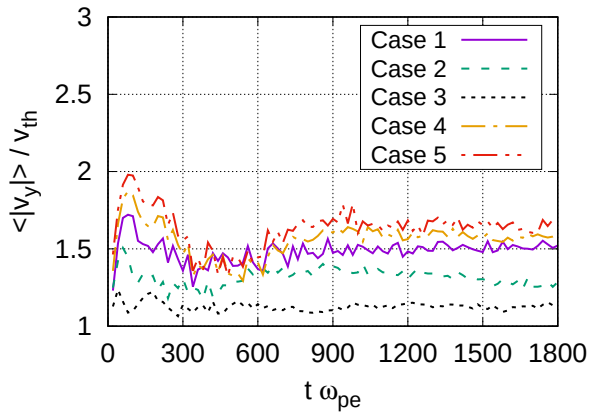

Fig. 10 Case 1 through 5: Average speed of v_y of electrons inside the beam region ($0 < x/\lambda_d < 20$, $-d_i/2 + \lambda_d < y < d_i/2 - \lambda_d$).